1 Aerogel Ring Imaging Čerenkov Counter

1.1 Physics Requirements

Identification of charged particles over the full kinematic range is one of the basic requirements for the upgraded Belle detector. The RICH, as described in this section, has been designed to separate kaons from pions over most of their momentum spectrum in the forward (endcap) part of the spectrometer,and to provide discriminaton between pions, muon and electrons below 1 GeV/c.

1.2 Detector Design Considerations

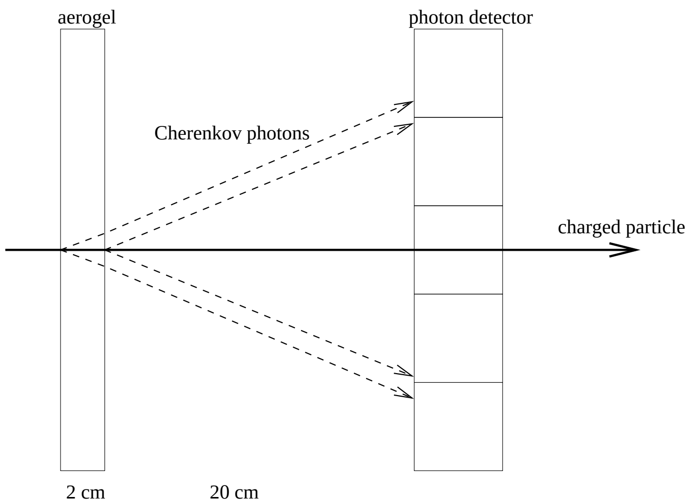

Fig. 1. *Proximity focusing RICH - principle*

The elements of the proximity focusing RICH counter are (Fig. 1):

- a *radiator* where Čerenkov photons are produced by charged particles,
- an *expansion volume* to allow Čerenkov photons to form rings on the photon detector surface,
- an array of *vacuum based position sensitive photon detectors*, that is capable of detecting single photons in a high magnetic field with high efficiency and with good resolution in two dimensions, and
- a *photon detector read-out system*.

The design choices are governed by the following criteria:

- To achieve the necessary performance, enough photons (about 10) have to be detected for each ring image at least for one of the particle species. This requirement fixes the length of the aerogel radiator to a few centimeters.

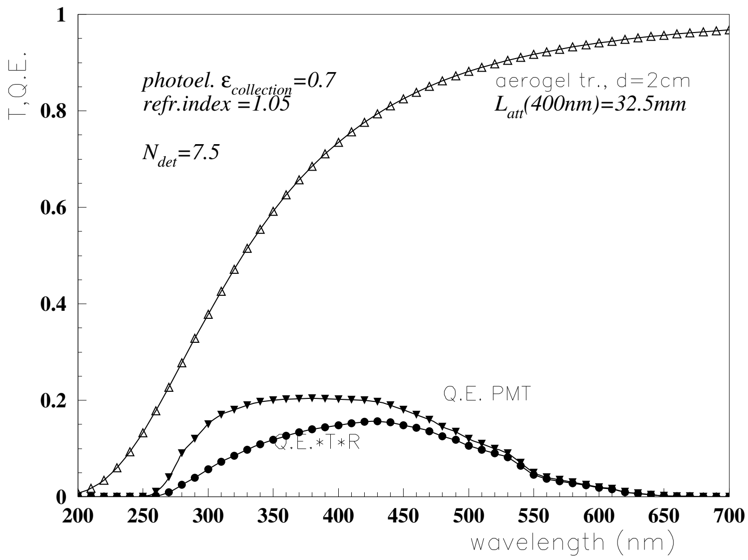

Fig. 2. *Transmission curve for the aerogel radiator (2 cm) [14] and the quantum efficiency of a typical multi-alkali PMT (H8500 [13]).*

- The required resolution in the measurement of the Čerenkov angle with such a photon detector is only achievable if the expansion gap is at about 20 cm, and the radiator thickness does not exceed a few centimeters, while the photon detector granularity is at about a few milimeters.

1.3 Radiator

The Čerenkov radiator is aerogel, a material which is already used in the present Belle ACC (Aerogel Cherenkov Counter). A plane with 2 cm thick radiator tiles is mounted perpendicularly to the beam direction. This radiator was chosen since it combines low mass and a low Čerenkov threshold. For aerogel with refractive index $n = 1.05$ the Čerenkov threshold momenta for pions is at 0.63 GeV/c, and the Čerenkov angle corresponding to $\beta = 1$ particles amounts to $\theta_c = 310\,\text{mrad}$. At 4 GeV/$c$, pions and kaons are separated by 23 mrad.

In Fig. 2 the transmission curve is shown for a typical 2 cm thick radiator sample. Since the losses of photons are dominated by Rayleigh scattering with a strong wavelength dependence (λ^{-4}) of the attenuation length Λ, the transmission varies considerably over the sensitive interval of a typical bi-alkali photocathode.

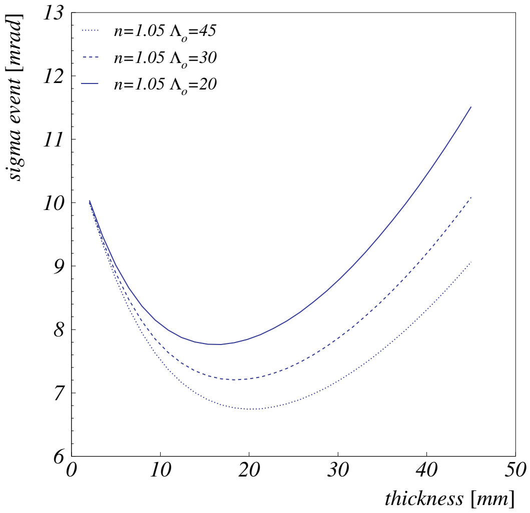

Fig. 3. *Čerenkov angle resolution per track $\sigma_\theta^{\mathrm{track}}$ as a function of the radiator thickness for three different attenuation lengths.*

The optimal radiator thickness was determined by ploting in Fig. 3 the figure of merit, resolution in Cherenkov angle measurement per track,

$$\sigma_\theta^{\mathrm{track}} = \frac{\sigma_\theta}{\sqrt{N_{pe}}},$$

which depends both on the resolution in Cherenkov angle measurement by a single photon σ_θ and on the number of detected photons N_{pe} (c.f. the R&D subsection, Fig. 11). The position of the minimum depends slightly on the transmission length. For a typical value of $\Lambda(400\ \mathrm{nm}) = 30$ mm, the best performance is achieved if the radiator thickness is around 20 mm.

Two possible tiling schemes of the aerogel radiator are shown in Fig. 4. One of the advantages of the hexagonal scheme is that the fraction of surface where the photon yield gets reduced due to tile edge effects is smaller (see Fig. 12). The hexagonal tiling needs three different tiles (full hexagon with 125 mm sides and two half-hexagons). The tiling with distorted squares needs three different tiles (one for each annulus), with a maximal side of about 220 mm.

1.4 Photon Detector

The position sensitive photon detector covers a surface of rougly 3.5 m^2, and is an essential component of the counter. The requirements for the photon detector are summarized as follows:

- Should be immune to the 1.5 T magnetic field,
- Should have single-photon sensitivity with a good single photon peak-to-valley ratio and high detection efficiency,

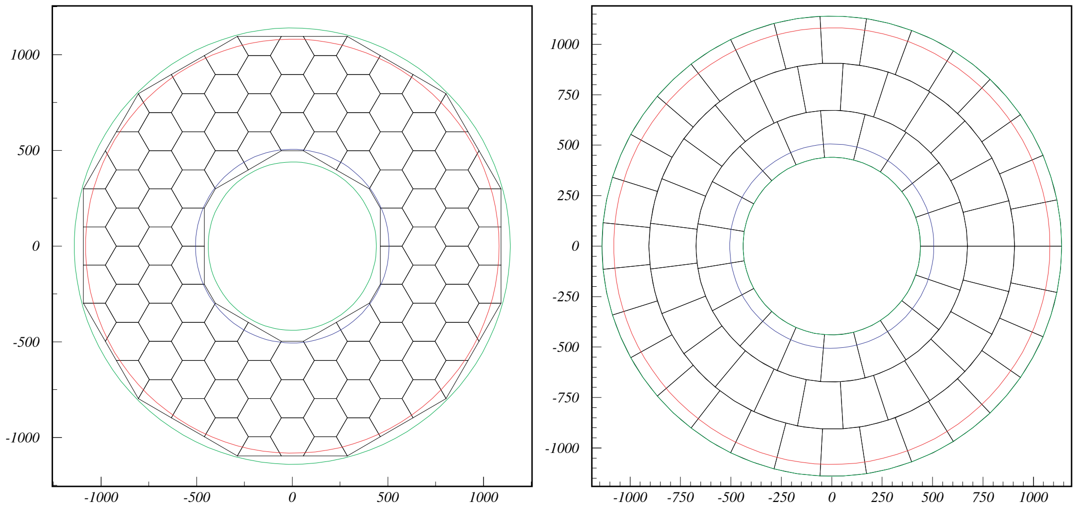

Fig. 4. *Two aerogel radiator tiling schemes.*

- Should have position resolution (RMS) of less than 2 mm,
- Should have high sensitivity for photons of $\lambda \approx 400$ nm (c.f. Fig. 2).

Currently we consider a proximity-focusing-type Hybrid Photo-Diode (HPD) or a Hybrid-Avalanche-Photo-Diode (HAPD) as the best candidate, since they have both excellent single-photon resolution and high detection efficiency even in high magnetic field. Some kinds of HPD's are already commercially available [10]. However, we can not use a focusing type HPD in the high magnetic field, and the effective area of the currently available proximity focusing type HPD is less than 50%. In order to enlarge the detection area of an HPD, we decided to develop with Hamamatsu Photonics K.K. (HPK) a new HPD of a proximity focusing type with pixel size of 5 mm square. Fig. 5 shows a schematic drawing of the H(A)PD, which has a housing of 72x72 mm^2 and 59x59 mm^2 sensitive area. This means 67% of the total area is covered by photo-diodes (PD) or avalanche PDs (APD). Four PD's or APD's, each with a 6x6 pixel array, are installed in a ceramic vessel as shown in Fig. 5, which leads to 12x12 pixels in total. The window is made of quartz and the photocathode material is multi-alkali.

A possible tiling scheme of the photon detector surface is shown in Fig. 6. The detector surface is covered with 600 HPD PMTs, with a 92% coverage.

1.5 Read-Out System

In parallel to the development of the photon detector, we are developing the readout electronics. Since the number of readout channels amounts to more than 80k in total, we need a special read-out scheme to treat them. We have therefore developed an ASIC which has the following properties:

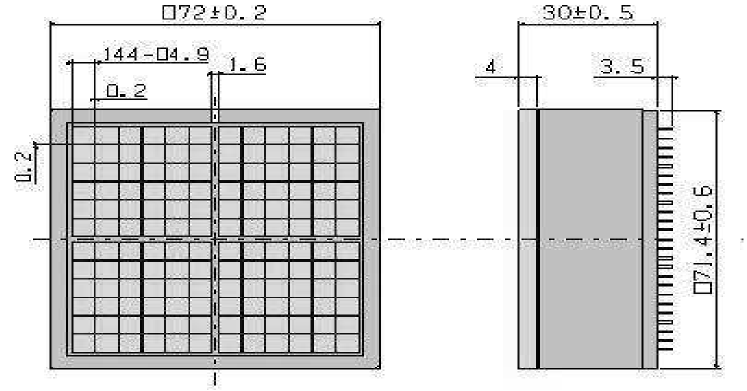

Fig. 5. *Schematics of the proximity focusing hybrid photon detector (HPD) under development.*

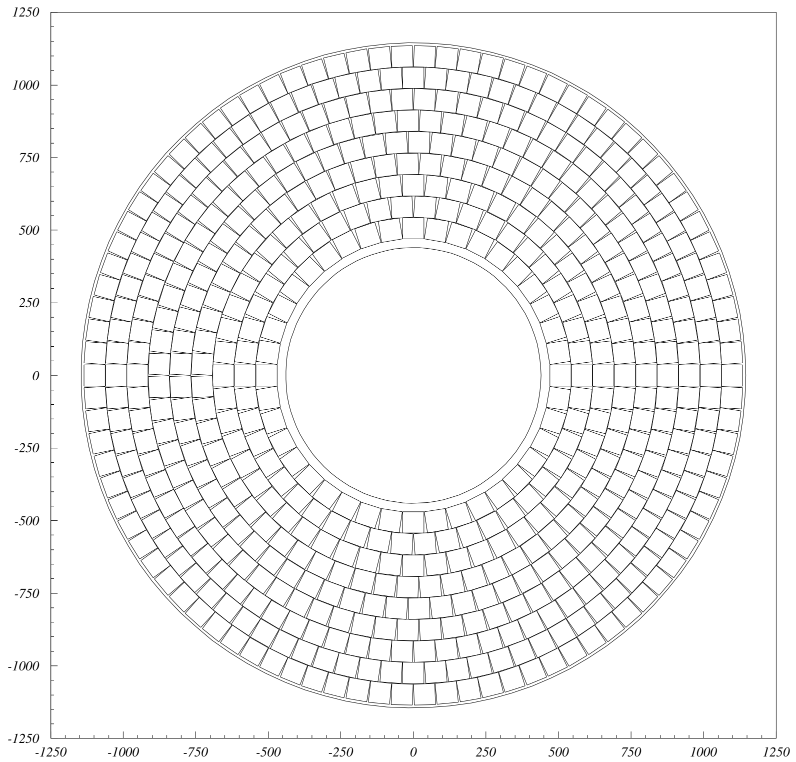

Fig. 6. *Photon detector tiling scheme.*

a) High gain with short shaping times, 5V/pC and 150 ns,
b) Variable gain amp to adjust the threshold, x 1-16,
c) Pipeline readout scheme with shift register,

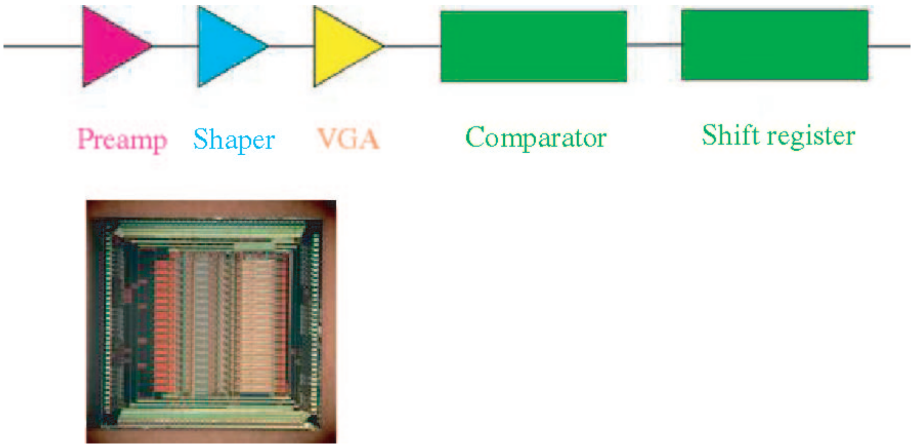

Fig. 7. *Schematic and photo of the ASIC (4.9x4.9 mm^2).*

d) Low power consumption, 5 mW/ch.

A schematic of the ASIC and a photo through microscope are shown in Fig. 7. Only the on/off information after the comparator are registered in the shift register. When a trigger signal is accepted, the last 4 bits of the shift register are duplicated in a 4-bits register, which is read out serially.

As a fall-back solution we could employ a low noise read-out system based on the type used in the Belle silicon vertex detector (SVD), but adapted to the special needs of a single photon detector with pads. The system, an upgrade of the integrated circuit used in the CleoIII RICH [19], employs two chips, VA64tap with preamplifiers, amplifiers and discriminators for 64 channels, and LS64 with a 64 channel logic level adaptor stage [20]. The full read-out chain of the chip could be designed in a very similar way as for the read-out for the SVD2 counter.

1.6 Expected performance

1.6.1 Number of photons

The expected number of Čerenkov photons was calculated by combining the measured values for quantum efficiency $\epsilon_q(\lambda)$ [13] and aerogel transmission $T(\lambda)$ (Fig. 2),

$$N_{phot} = 370\mathrm{cm}^{-1}\, d\, \epsilon_e\, \epsilon_a\, \epsilon_t\, \sin^2\theta_c \int \epsilon_q(\lambda)\, T(\lambda)\, \lambda^{-2}\, d\lambda, \tag{1}$$

where d is the radiator thickness (2 cm), ϵ_e is the single photo-electron pulse detection efficiency (estimated to be 0.70 for the HPD), and ϵ_a is the active surface fraction of the photon detector surface (0.67 in the case of HPD);

$\epsilon_t = 0.92$ is the fraction of the surface covered with photon detector modules in a particular tiling scheme (Fig. 6). The resulting expected number of detected Čerenkov photons is 7.5.

1.6.2 Resolution of the RICH

From the photon hit coordinate as measured by the photon detector and from the particle trajectory as given by the tracking chamber, the photon direction is reconstructed to obtain the Čerenkov angle and thus the velocity βc of the particle. Sources of error in the measurement by a single photon are as follows. The finite radiator thickness, $d = 2$ cm, contributes $\sigma_\theta^{emp} = d/(\ell\sqrt{12}) \sin\theta_c \cos\theta_c = 8.4$ mrad. The second contribution comes from the finite coordinate resolution of the photon detector $\sigma_\theta^{pix} = a/(\ell\sqrt{12}) \cos^2\theta_c = 6.4$ mrad, with a pad size of $a = 4.9$ mm and the radiator to photon detector distance of $\ell = 20$ cm. The chromatic error, a consequence of dispersion, the variation of the refractive index over the energy range of those Čerenkov photons that are detected by the photon detector, is determined from the measured variation of refractive index with wavelength, the transmission of aerogel and the photo-detector quantum efficiency (Fig. 2). From the resulting R.M.S. spread σ_n in refractive index we calculate $\sigma_\theta^{dis} = \sigma_n/(n \tan\theta_c) = 2?$ mrad . From the experience with the HERMES RICH [7] we conclude that the contribution due to the imperfections and inhomogenuity of the radiator can be estimated at 2 mrad. Finally, the contribution arising from the error in track parameters as determined by the tracking system and extrapolated to the radiator is expected to amount to $\sigma_\theta^{tr} = 5$ mrad$/(p/\mathrm{GeV}/c)$.

The combined single photon error is finally obtained by summing the above errors in squares. For 4 GeV/c momentum tracks it amounts to $\sigma_\theta = 11$ mrad. Assuming 7.5 detected photons for a $\beta = 1$ particle, the measurement precision is

$$\sigma_\theta^{(N)} = \frac{\sigma_\theta}{\sqrt{N}} = 4 \text{ mrad.} \tag{2}$$

In absence of backgrounds, the proposed counter would thus enable a 5σ pion-kaon separation at the kinematic limit of 4 GeV/c. Pions would be separated at a 4σ level from electrons up to about 1 GeV/c.

1.6.3 Background

Since the number of photons per ring is rather low, backgrounds could degrade the performance as discussed above. The following sources of background expected in the RICH photon detector were considered:

1. Rayleigh scattered Čerenkov photons from the same track.
2. Čerenkov photons emitted by the same track in the photon detector window.
3. Čerenkov photons emitted by other charged tracks in the event.
4. Čerenkov photons emitted by products of primary photon conversion in the material in front of the RICH radiator and in the radiator itself.
5. Beam related background hits.
6. Electronic noise.

The levels of backgrounds (1) and (2) were estimated from the test beam data (c.f. the R&D subsection, Fig. 10a), and turned out to be the dominant source.

The levels of backgrounds (3) and (4) were studied by computer simulation. Because of a rather small diameter of Čerenkov rings (12 cm) as compared to the typicall distance between track impact points on the aerogel radiator, the background (3) does not contribute significantly.

The level of source (5) was estimated from the current background rate in the endcap ACC, and scaled by a factor of 20 as expected from the luminosity increase. This rough estimate yields values from 60 Hz/cm^2 to 140 Hz/cm^2 for the modules at the maximum and minimum radial distance from the beam. Finally, the electronic noise is estimated by assuming a conservative value of 10^{-3} for the probability of a noise hit.

In total, we expect 0.7 smoothly distributed background hits within the annulus of $\pm 3\sigma_\theta$ of the 4 GeV/c pion ring.

1.6.4 Particle identification capabilities

The particle identification capabilities of the counter were evaluated by using simulated data. The backgrounds which are not included in simulation (sources 1,2,5,6) were generated according to observed or expected rates.

1.7 R&D Results

Aerogel radiator

The hydrophobic aerogel with a low refractive index ($n = 1.01 \sim 1.03$), as developed for the Belle-ACC, is characterized by a high transmission length (~ 40 mm at a wave length of 400 nm). However, the transmission length of aerogel with a higher refractive index of $n = 1.05$ fell below one half the value compared to the aerogel with $n = 1.03$. Keeping in mind that for a collider experiment a hydrophobic aerogel is preferred to a hydrophilic one, we reex-

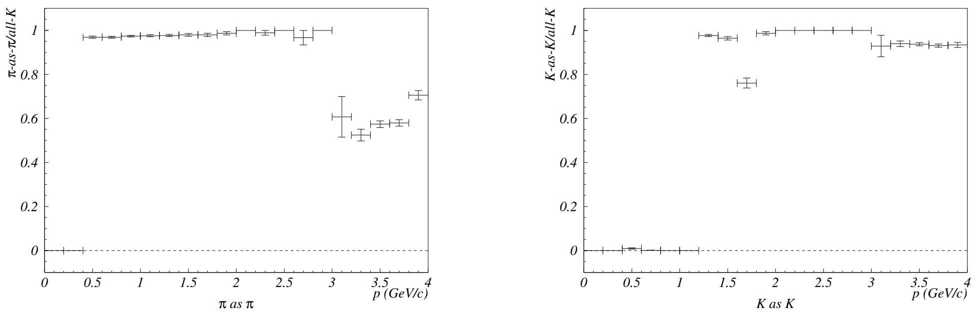

Fig. 8. *Particle identification capabilities of the aerogel RICH counter: pion identification efficiencies at 5% kaon misidentification probability (left); kaon efficiency at 5% pion misidentification probability (right).*

amined the hydrophobic aerogel production technique in a joint development with Matsushita Electric Works Ltd.

As a result, we found that the important factors determining the transmission length are the solvent and selection of the precursor to be used for its production. Originally, we used methyl-alcohol for the solvent, and methyl-silicate as a precursor [5]. When we applied di-methyl-formamide (DMF) [16], and changed the supplier of the precursor, we could improve considerably the transmission length of the aerogel. Fig. 9 shows the refractive indices of aero-

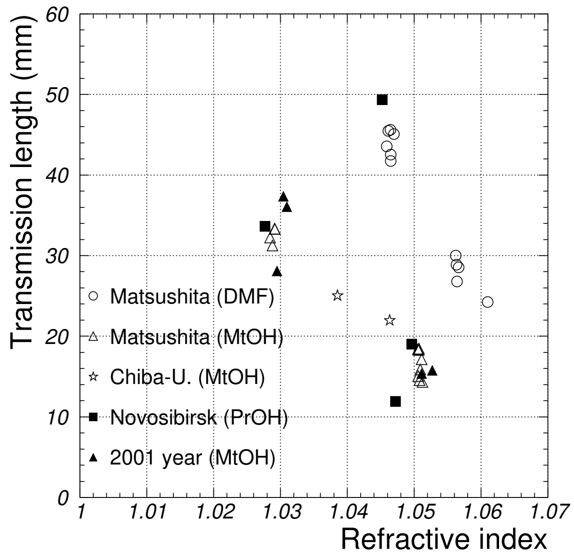

Fig. 9. *Transmission length at 400 nm and refractive index at 405 nm for the aerogel samples used in the test.*

gel and the relation to transmission length for samples which were used in the beam test. The Matsushita(DMF) samples are clearly superior to other hydrophobic aerogels.

System test

In a series of beam tests we have checked the performance of a complete system. While in the first test [11] at the KEK-PS $\pi 2$ beam line an array of multi-anode PMTs (Hamamatsu R5900-M16) was used for photo-detection, the recently developed flat-panel PMTs, Hamamatsu H8500, were employed in the second one [12]. 16 PMTs were used in a 4×4 array and aligned with a 52.5 mm pitch, with an effective area of photon detection of 84%. At the back of each PMT, an analog memory board is attached to read out multi-channel PMT signals.

Most of the test measurements were performed with a π^- beam at 3 GeV/c. To systematically evaluate the detector performance, data were taken with different aerogel samples with various transmission lengths and thicknesses. Data were also taken by varying the π^- momentum in the range from 0.5 GeV/c to 4.0 GeV/c.

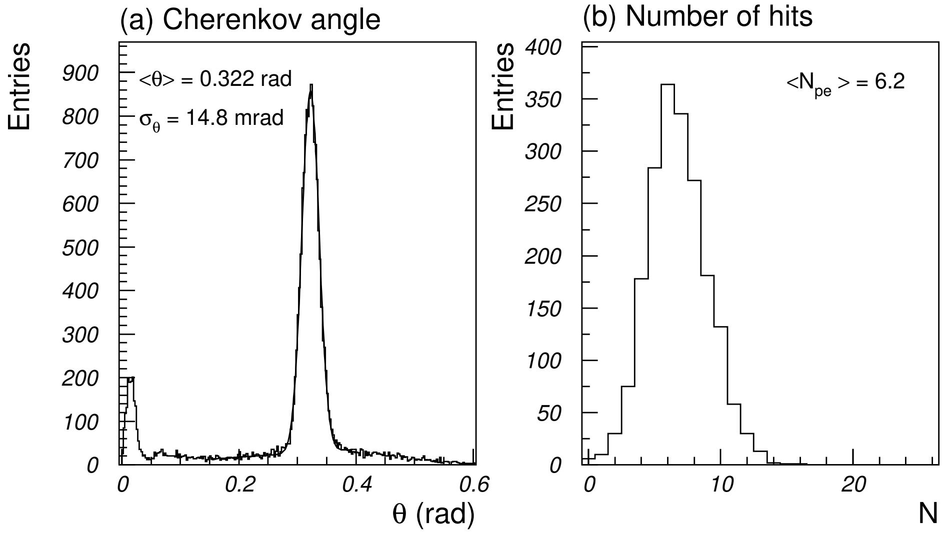

Fig. 10. *Distribution over the Cherenkov angle for single photons (a), and the number of detected photons per ring (b), for a* 20 *mm thick aerogel radiator sample with* $n = 1.056$ *and a transmission length of* 30 *mm.*

Fig. 10a shows a typical distribution of the Cherenkov-angle for single photons. Cherenkov photons from the aerogel radiator are clearly seen with a low background level. The flat background hit distribution on the photon detector is consistent with the assumption that it originates from Cherenkov photons which were Rayleigh scattered in the radiator. The peak at small Cherenkov angles is due to Cherenkov radiation generated by the beam particle in the

PMT window.

Cherenkov-angle resolution for single photons

The angular resolution was obtained from a fit of the Cherenkov angle distribution (Fig.10a) with a Gaussian signal and a linear function for the background. The resolution was typically around 14 mrad, independent of the refractive index. The main contributions to the resolution of the Cherenkov angle come from the uncertainty in the emission point and from the pixel size of the PMT. The measured variation of the resolution with the thickness of aerogel is shown in Fig. 11 together with the expectations. The measured resolution the expected values matches reasonably well, appart from a discrepancy between the two, which could be accounted for by a constant additional contribution of about 6 mrad. The discrepancy could arise from the effect of aerogel (non-flat aerogel surface and possible non-uniformities in the refractive index due to position variation and chromatic dispersion), which are subject to further investigation.

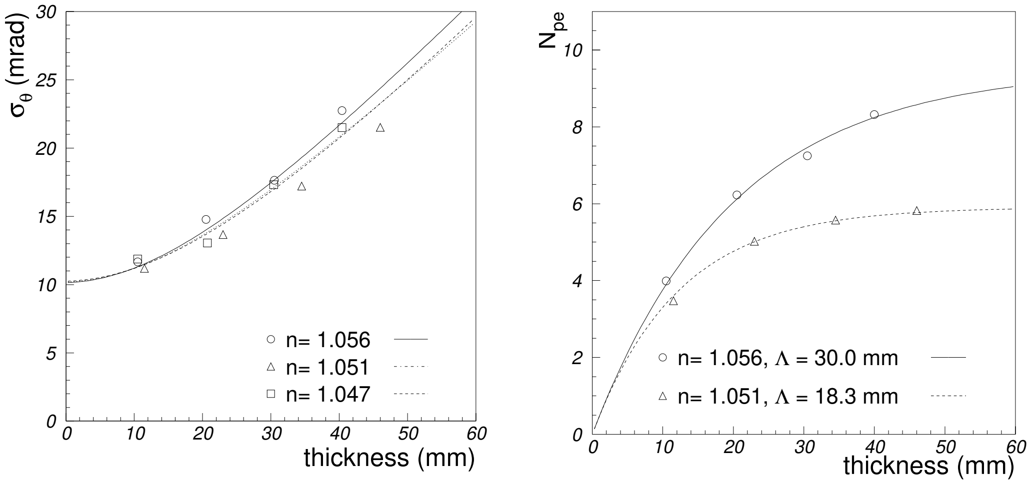

Fig. 11. *Angular resolution (left) and the number of detected photons per Cherenkov ring as a function of the aerogel thickness. The symbols correspond to the data recorded with different aerogel samples.*

Photoelectron yield

Fig. 10b shows a typical distribution of the number of hits within $\pm 3\sigma$ from the average Cherenkov angle. The number of hits for the signal region was estimated by subtracting the background from the fits to the Cherenkov-angle distribution. Fig. 11 shows the dependence of the number of detected photons on the aerogel thickness. As expected, the number of photons does not linearly increase with the aerogel thickness, but saturates due to the scattering effect

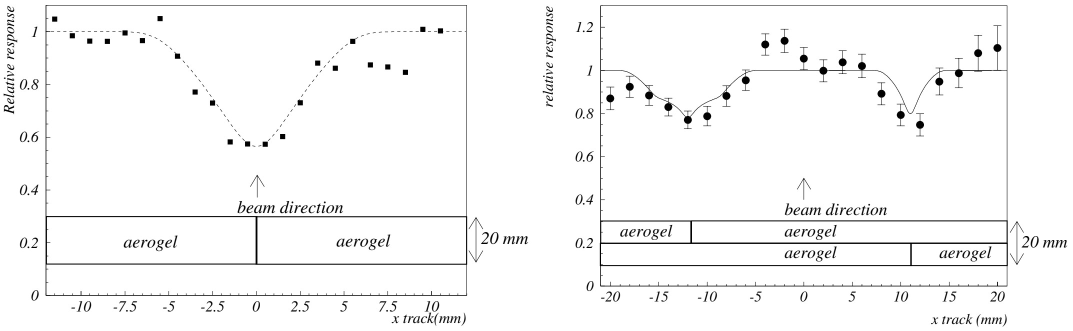

Fig. 12. *The number of Cherenkov photons detected on the ring, as a function of the charged particle impact point position on the aerogel tile. The values shown are normalized to the measured values in case of a single tile covering the full range. Also shown is the estimate of a simple model.*

in aerogel. For pions with momenta above 1 GeV/c, the number of detected Cherenkov photons was typically around 6 for aerogel samples with $n = 1.05$. The deviation from the expected value (about 9) can be accounted for by the rather early development stage of the employed PMT tubes. In fact, if normalized to the best tubes in the second delivery batch, the yield per ring is very close to the expected value.

It has been already noted by the HERMES group [7] that a loss of Cherenkov photons occurs at the side wall boundaries between adjacent aerogel tiles. We have confirmed this finding by measuring the number of photons on the Cherenkov ring as a function of the distance of the charged particle impact point from the boundary between two tiles. The measurement is shown in Fig. 12, where a dip is seen at the tile boundaries for two different tiling schemes. In order to eliminate other geometrical factors, like for example the acceptance of the photon detector, the measured yield was normalized to the yield obtained with one tile covering the entire range. The result clearly indicates a reduction of yield when the charged particle is closer than about 5 mm to the boundary of a 2 cm thick aerogel tile. It is worth noting that a simple model, where all photons hitting the boundary between the two tiles get lost, accounts for most of the observed dependence. From the result it is clear that the tile size should be as large as possible to reduce the impact of the loss.

Particle Identification

Finally, we estimate the performance of pion/kaon separation in the momentum range of around 4 GeV/c. If we take into account a typical measured value for the single-photon angular resolution, $\sigma_c \sim 14$ mrad, and the number of detected photons $N_{pe} \sim 6$, typical for 20 mm thick aerogel samples with $n = 1.05$, we can estimate the Cherenkov angle resolution per track to be $\sigma_c/\sqrt{N_{pe}} =$ 5.7 mrad. This naive estimate is also confirmed by the direct measurement shown in Fig. 13. Here, the track-by-track Cherenkov angle is

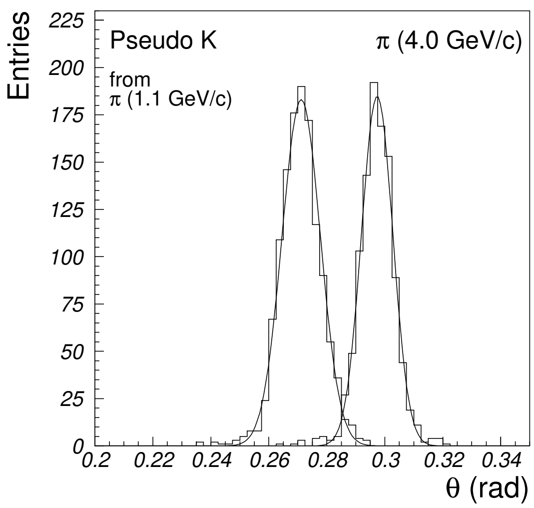

Fig. 13. *Cherenkov angle per track for pions of* 4.0 GeV/c *and* 1.1 GeV/c. *Pions at* 1.1 GeV/c *are used to represent the kaon beam of* 4 GeV/c. *The angular resolutions for* 4.0 GeV/c *and* 1.1 GeV/c *are* 5.4 *mrad and* 6.7 *mrad and two peaks are separated by* 4.2σ.

calculated by taking the average of the angles measured for hits around the predicted position of the Cherenkov ring. From this we can deduce that at 4 GeV/c, where the difference of Cherenkov angles for pions and kaons is 23 mrad, a 4σ separation between the two is possible. As an additional cross check, we have also collected data with the pion beam of 1.1 GeV/c, which can be used to represent a kaon beam of 4 GeV/c (apart from a slightly larger sigma due to multiple scattering). As can be seen from Fig. 13, the two peaks are well separated.

HPD development

Although the system test was very successful, there are still several issues which have to be solved for implementation in the Belle spectrometer. The most important item is the development of a PMT which can be operated in a high magnetic field (1.5 T). In order to confirm the ability of candidate photon detectors HPD and HAPD to efficiently detect single photons over a large active area, a single channel HPD and a 3x3 multi-channel HAPD were tested by using a laser diode light pulser ($\lambda = 850$ nm). Fig. 14 shows a multi-photon spectrum obtained by a HPD, which was operated at 8 kV for electron bombardment (EB) (typical EB gain was 1500) and 80 V for bias. The leak current was 4 nA and the detector capacitance was 20 pF.

Multi-photon spectrum was obtained also by the HAPD prototype (Fig. 15). The gain was higher ($2.6 \cdot 10^4$) in the case of the HAPD due to the avalanche

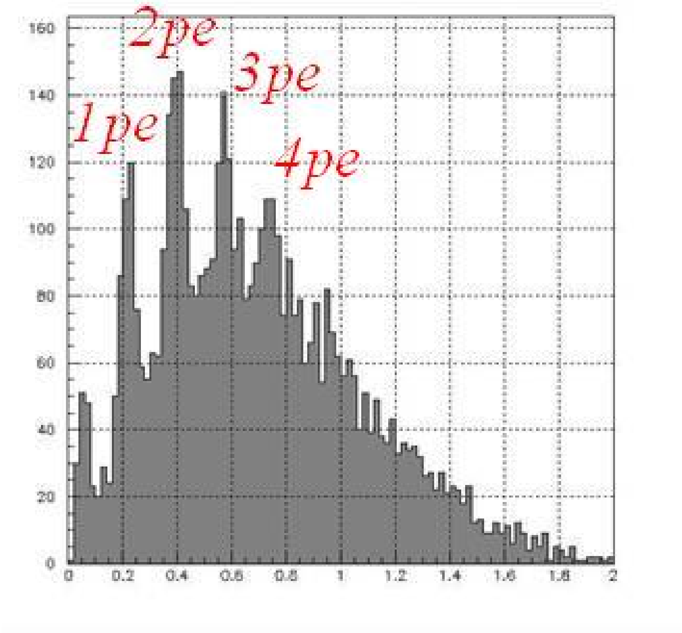

Fig. 14. *Multi-photon spectrum obtained by the single-channel HPD.*

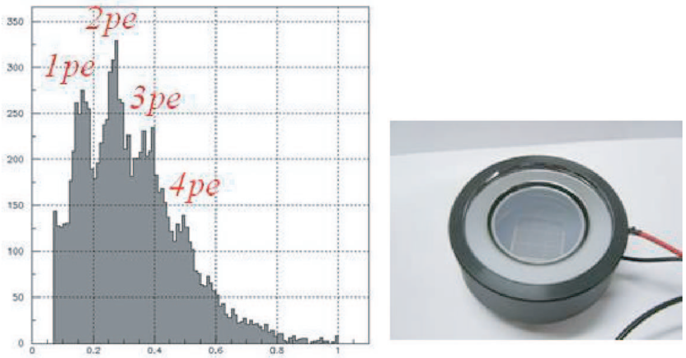

Fig. 15. *Multi-photon spectrum obtained by the 3x3 multi-channel HAPD and a photo of the HAPD.*

gain of about 15. However, the detector capacitance was 73 pF and the leak current amounted to 14 nA, resulting in a worse signal to noise ratio than in the case of the HPD. Although both the HPD and the HAPD have shown an excellent performance, the HPD gives a slightly better resolution.

Prototype production of APD's and PD's is going on in HPK, and evaluation of the samples is being carried out. While so far there are no serious problems for the PD's except for a slightly worse timing response, a large leak current was observed in APD's after the activation of photocathode. Futhermore larger noise than expected is seen in APD's. Hamamatsu Photonics is investigating the HAPD's to solve this problem in the next batch. A delivery of prototype 12x12 channel HAPD's is expected in January 2004, and a beam test is planned for February.

References

[1] M.Cantin et al. Nucl. Instr. Meth. **118** (1974) 177.

[2] A.Abashian et al., Nucl. Instr. and Meth. A **479** (2002) 117.

[3] T.Sumiyoshi et al., Nucl. Instr. and Meth. A **433** (1999) 385.

[4] T.Iijima et al., Nucl. Instr. and Meth. A **453** (2000) 321.

[5] I. Adachi et al., Nucl. Instr. and Meth. A **355** (1995) 390390; T. Sumiyoshi et al., J. Non-Cryst. Solids **225** (1998) 369.

[6] D.E.Fields et al. Nucl. Instr. Meth. A **349** (1994) 431.

[7] N.Akopov et al. Nucl. Instr. Meth. A **479**(2002) 511.

[8] T.Ypsilantis and J.Seguinot, Nucl. Instr. Meth. A **368** (1995) 229.

[9] T.Iijima, "Aerogel Cherenkov Counter in Imaging Mode", JPS Meeting, Tokyo Metropolitan University, September 1997.

[10] DEP catalog

[11] I. Adachi et al., "Test of a proximity focusing RICH with aerogel as radiator", Proceedings for the IEEE Nuclear Science Symposium, Norfolk, VA, November 10-15, 2002; hep-ex/0303038; T.Iijima et al., Nucl. Instr. Meth. A **502** (2003) 231.

[12] T. Matsumoto et al., to be published in NIM A; physics/0309032.

[13] H8500 data sheet, Hamamatsu Photonics K.K.

[14] aerogel transmission

[15] Hamamatsu Photonics K.K.

[16] Matsushita Electric Works Ltd. has a Japanese patent (No. 2659155) for usage of DMF as solvent to make aerogel.

[17] A.R. Buzykaev et al. Nucl. Instr. Meth. A **433** (1999) 396.

[18] H.Ikeda et al. Nucl. Instr. Meth. A **372** (1996) 125.

[19] M. Artuso et al., Nucl. Instr. Meth. A **502** (2003) 91.

[20] Ideas SA, Oslo.